Acta Neuropathologica
Communications

Neuronal *SNCA* transcription during Lewy body formation

Tomoya Kon[1,2], Shelley L. Forrest[1,3,4], Seojin Lee[1], Ivan Martinez-Valbuena[1], Jun Li[1], Nasna Nassir[5,6],
Mohammed J. Uddin[5,6], Anthony E. Lang[1,7,8] and Gabor G. Kovacs[1,3,4,7,8,9]*

Abstract

Misfolded α-synuclein (α-syn) is believed to contribute to neurodegeneration in Lewy body disease (LBD) based on considerable evidence including a gene-dosage effect observed in relation to point mutations and multiplication of *SNCA* in familial Parkinson's disease. A contradictory concept proposes early loss of the physiological α-syn as the major driver of neurodegeneration. There is a paucity of data on *SNCA* transcripts in various α-syn immunoreactive cytopathologies. Here, the total cell body, nuclear, and cytoplasmic area density of *SNCA* transcripts in neurons without and with various α-syn immunoreactive cytopathologies in the substantia nigra and amygdala in autopsy cases of LBD (n = 5) were evaluated using RNAscope combined with immunofluorescence for disease-associated α-syn. Single-nucleus RNA sequencing was performed to elucidate cell-type specific *SNCA* expression in non-diseased frontal cortex (n = 3). *SNCA* transcripts were observed in the neuronal nucleus and cytoplasm in neurons without α-syn, those containing punctate α-syn immunoreactivity, irregular-shaped compact inclusion, and brainstem-type and cortical-type LBs. However, *SNCA* transcripts were only rarely found in the α-syn immunoreactive LB areas. The total cell body *SNCA* transcript area densities in neurons with punctate α-syn immunoreactivity were preserved but were significantly reduced in neurons with compact α-syn inclusions both in the substantia nigra and amygdala. This reduction was also observed in the cytoplasm but not in the nucleus. Only single *SNCA* transcripts were detected in astrocytes with or without disease-associated α-syn immunoreactivity in the amygdala. Single-nucleus RNA sequencing revealed that excitatory and inhibitory neurons, oligodendrocyte progenitor cells, oligodendrocytes, and homeostatic microglia expressed *SNCA* transcripts, while expression was largely absent in astrocytes and microglia. The preserved cellular *SNCA* expression in the more abundant non-Lewy body type α-syn cytopathologies might provide a pool for local protein production that can aggregate and serve as a seed for misfolded α-syn. Successful segregation of disease-associated α-syn is associated with the exhaustion of *SNCA* production in the terminal cytopathology, the Lewy body. Our observations inform therapy development focusing on targeting *SNCA* transcription in LBD.

Keywords α-Synuclein, Lewy body disease, mRNA, Parkinson's disease, Proteinopathy, Proteinopenia, RNAscope, Single-nucleus RNA sequencing, *SNCA*, Transcript

*Correspondence:
Gabor G. Kovacs
Gabor.Kovacs@uhn.ca
Full list of author information is available at the end of the article

Kon *et al. Acta Neuropathologica Communications*   (2023) 11:185

Page 2 of 17

Introduction

Lewy body disease (LBD) is characterized by the presence of Lewy bodies (LBs) composed of α-synuclein (α-syn) [27, 31, 35, 73]. α-Syn is a neuronal cytoplasmic and pre-synaptic protein encoded by *SNCA* gene, which was originally described in the pre-synaptic terminal and nucleus of neurons from Torpedo californica [47]. A conformational change, termed also as misfolding, gives rise to the emergence of an aggregation nucleus composed of α-syn, commonly referred to as a seed [27, 31]. This seed possesses the capacity to actively engage endogenous monomeric α-syn molecules and instigate their aggregation process [48, 49, 61]. The application of α-syn immunohistochemistry allowed the detection of non-LB type cytopathologies that are more abundant than classical LBs. In addition, it suggested that the maturation process of classical LB formation encompasses sequential stages [27, 33, 40, 73]. Importantly, cell culture and animal studies [13, 15, 46, 54, 59] also showed a similar process. Accordingly, the initial phase of this process is characterized by the presence of punctate (or diffuse) α-syn immunoreactivity (IR) in the cytoplasm, which shows negative IR for both ubiquitin and p62 antibodies. Subsequently, irregular-shaped compact inclusions considered to be analogous to the pale bodies observed in the HE-staining, which exhibit IR against ubiquitin and p62 antibodies, are generated. Ultimately, the progression leads to the formation of fully mature classical LBs characterized by a central round core surrounded by a halo [27, 35, 40, 73].

Rare point mutations and multiplications (duplication and triplication) of *SNCA* lead to familial Parkinson's disease leading to the hypothesis of a gene-dosage effect [23, 26, 50, 58]. Many studies support the notion that accumulation of misfolded α-syn drives disease pathogenesis ('proteinopathy') [8, 27, 31, 35, 37, 48, 49, 59, 73]. Therefore, α-syn is currently a major therapeutic target for synucleinopathies, for example by eliminating pathological aggregates by monoclonal α-syn antibodies, by inhibiting α-syn aggregation, or by stabilizing α-syn monomers, or by directly targeting *SNCA* gene expression with miRNA and antisense oligonucleotide therapies, amongst others [42, 55, 65]. However, it has been argued that as proteins aggregate, their soluble protein pool becomes depleted (referred to as 'proteinopenia') and this event is a major contributor to the neurodegeneration in LBD [21, 22], supported in part by the absence of notable impact in recent clinical trials involving monoclonal α-syn antibodies [42, 55]. These two divergent concepts dictate completely opposing strategies for disease-modifying treatment, specifically the eradication of disease-associated α-syn or the early replacement of normal physiological α-syn.

SNCA expression in the substantia nigra (SN) in LBD has been reported to be both up- and down-regulated compared with controls [5, 7, 12, 14, 16, 28, 34, 53, 56, 60, 69]. However, these studies did not compare *SNCA* transcription with or without α-syn pathology because tissue digestion methods were used. Elucidation of *SNCA* transcriptional regulation during LB formation process is crucial for understanding the pathogenesis and progression of LBD, and for guiding the strategy for molecular therapy. Here, we report the process of cellular *SNCA* transcription during LB formation using RNAscope combined with immunofluorescence for disease-associated α-syn, complemented by single-nucleus RNA sequencing (snRNA-seq) to map the cell population showing *SNCA* transcripts.

Methods

Cases and tissue preparation

Formalin-fixed paraffin-embedded 4-µm thick sections were investigated. For RNAscope, sections were trimmed to approximately 1.5 cm × 1.5 cm in size from the substantia nigra (SN, n = 5 in LBD cases, n = 2 in controls; patients without neurodegenerative pathology), amygdala (n = 3 in LBD, n = 2 in control cases). To compare nuclear and cytoplasmic *SNCA* transcripts, pons (n = 2 in control cases) was also investigated. For immunohistochemistry, midbrain, basal ganglia, and amygdala were analyzed (n = 5 each in cases of LBD and controls; for details see Additional file 1). In addition, flash-frozen frontal cortex from 3 control cases stored at −80 °C were also used for snRNA-seq analysis. A total of 13 (5 LBD and 8 control) cases were included in this study (Table 1). Non-diseased control samples were used only to demonstrate the presence of *SNCA* transcripts in cells and to compare nuclear and cytoplasmic transcripts. All cases had a routine neuropathological assessment based on the current consensus criteria including Braak LBD stage [8], Lewy pathology consensus criteria [4], and Alzheimer's disease neuropathological change (ADNC) [51].

RNAscope with immunofluorescence

RNAscope assay with immunofluorescence was performed as previously reported [25]. Briefly, endogenous peroxidase was quenched by RNAscope Hydrogen Peroxide Solution (ACD) for 10 min, and sections were pretreated with RNAscope Target Retrieval reagent (ACD) for 30 min at 99 °C before applying RNAscope Protease Plus (ACD) for 30 min at 40 °C. Sections were incubated with probe mixtures for 2 h at 40 °C. C1 probe designates *SNCA* (ACD, Cat no. 421311, targeted regions 291–3084 bp, accession number NM_001146054.1) and

Table 1 Case demographics, regions, antibodies, and probes used in the study

Case	Age	Sex	PMI, hours	Clinical phenotypes	Pathological diagnosis	Braak LBD stage[8]	Regions and probes used for RNAscope	Region and antibodies used for IHC	Region used for single-nucleus RNA sequencing
1	73	F	n.a	PD	LBD	4	SN (*SNCA, RBFOX3*), amygdala (*SNCA, RBFOX3, ALDH1L1*)	SN, basal ganglia, amygdala (SYN-1, 5G4)	–
2	62	F	15	PDD	LBD	5	SN (*SNCA, RBFOX3*), amygdala (*SNCA, RBFOX3, ALDH1L1*)	SN, basal ganglia, amygdala (SYN-1, 5G4)	–
3	81	M	< 24	PDD	LBD	5	SN (*SNCA, RBFOX3*), amygdala (*SNCA, RBFOX3, ALDH1L1*)	SN, basal ganglia, amygdala (SYN-1, 5G4)	–
4	62	M	4	PD	LBD	4	SN (*SNCA, RBFOX3*)	SN, basal ganglia, amygdala (SYN-1, 5G4)	–
5	85	M	n.a	PD	LBD	4	SN (*SNCA, RBFOX3*)	SN, basal ganglia, amygdala (SYN-1, 5G4)	–
6	52	F	38	–	Control	None	SN (*SNCA, RBFOX3*), amygdala (*SNCA, RBFOX3, ALDH1L1*), pons (*SNCA, Olig2*)	SN, basal ganglia, amygdala (SYN-1, 5G4)	–
7	64	F	n.a	–	Control	None	SN (*SNCA, RBFOX3*), amygdala (*SNCA, RBFOX3, ALDH1L1*), pons (*SNCA, Olig2*)	SN, basal ganglia, amygdala (SYN-1, 5G4)	–
8	66	M	12	–	Control	None	–	SN, basal ganglia, amygdala (SYN-1, 5G4)	–
9	66	M	20	–	Control	None	–	SN, basal ganglia, amygdala (SYN-1, 5G4)	–
10	75	M	30	–	Control	None	–	SN, basal ganglia, amygdala (SYN-1, 5G4)	–
11	74	M	12.5	–	Control	None	–	–	Frontal cortex
12	74	M	6.3	–	Control	None	–	–	Frontal cortex
13	77	M	4	–	Control	None	–	–	Frontal cortex

IHC immunohistochemistry; *LBD* Lewy body disease; *LPC* Lewy pathology consensus criteria; *n.a.* not available; *PD* Parkinson's disease; *PDD* Parkinson's disease dementia; *PMI* postmortem interval; *SN* substantia nigra

was detected with Opal 570 fluorophore (1:750). C2 probe labeled *Olig2* for an oligodendrocyte maker (ACD, Cat no. 424191-C2, target regions 929–2502 bp, accession number NM_005806.3), C3 probe was assigned for *ALDH1L1* for a marker of astrocytes (ACD, Cat no. 438881-C3, targeted regions 1999–2982 bp, accession number NM_001270364.1), and C4 probe was set for *RBFOX3* for a neuronal marker (ACD, Cat no. 415591-C4, targeted regions 720–2217 bp, accession number NM_001082575.2). Cell-type-specific probes were detected with the Opal 690 fluorophore (1:750). After probe hybridization, the slides were washed and hybridized, and developed with an RNAscope Multiplex Fluorescent V2 Assay kit. The slides from the midbrain and amygdala were further processed for

immunofluorescence using phosphorylated α-syn antibody (clone #64, 1:5000, Wako, Osaka, Japan) for 1 h incubation at room temperature (RT). To evaluate astrocytic α-syn pathology that is undetectable using phosphorylated α-syn antibodies, for selected amygdala sections, we used the 5G4 α-syn antibody (1:100) for 1 h incubation at RT [37, 39]. Eighty-percent formic acid for 5 min was added before the process of RNAscope protease plus for 5G4 α-syn antibody. Based on a pilot-fashion testing, this protocol proved to be the most efficient to show 5G4 IR pathology with preserved *SNCA* transcripts. After washes, the sections were incubated with Alexa 488-conjugated donkey anti-mouse antibody (1:500, Invitrogen/ThermoFisher) for 1 h at RT and mounted with 4′,6-diamidino-2-phenylindole (DAPI) with mounting

Kon *et al. Acta Neuropathologica Communications*　　(2023) 11:185

Page 4 of 17

medium. The regions, probes, and antibodies used in the study were summarized in Table 1.

Acquisition of images

Acquisition of images was performed using Nikon C2Si+confocal on a Nikon Ti2-E inverted microscope equipped with a 40X objective lens for a single stack (NA: 0.95). Appropriate filter settings were used as follows; DAPI, excitation 405 nm, emission 400–720 nm; Alexa 488, excitation 488 nm, emission 430–500 nm; Opal 590, excitation 561 nm, emission 520–600 nm; Opal 690, excitation 640 nm, emission 620–720 nm. Single-stack images were captured using the NIS-Elements AR software (version 5.30.04). Only a few selected sections were also captured with a 100X objective lens for the acquisition of a z-stack of slices, where the inter-slice distance was 0.1 μm. Subsequently, a three-dimensional image was generated utilizing the NIS-Elements AR software in these selected sections. The parameters for taking pictures were standardized and maintained throughout the entire experiment.

Morphometry

We identified the cells with cell-specific markers for neurons, oligodendrocytes, and astrocytes using cell-specific probes. The region of interest (ROI) for the cell body, nuclear, and LB area was manually delineated using the cell-specific markers and DAPI signal positivity (see Additional file 1: Fig. S1). First, the Lookup Table (LUT) strength of the cell-specific marker and DAPI channels was increased sufficiently to enhance the visibility of autofluorescence from neuromelanin and/or lipofuscin pigments (see Additional file 1: Fig. S1B). The borders of the cell body were then traced based on these signals as total cell body area (see Additional file 1: Fig. S1C). Subsequently, DAPI channel was selected, and the nuclear edge was outlined as the nucleus area (see Additional file 1: Fig. S1D). Phosphorylated-α-syn immunostaining channel was chosen and the edge of LB is drawn as LB area (see Additional file 1: Fig. S1E). Finally, the LUT parameters were restored to normal settings and the NIS-Elements software captured the area positive for *SNCA* transcripts above the threshold within the ROI (see Additional file 1: Fig. S1F). Following our previous report [25], a capture threshold for *SNCA* transcripts fluorescence intensity that exceeded the autofluorescence level was established (see Additional file 1: Fig. S1F). This criterion ensured independence from the potential impact of autofluorescence during analysis. *SNCA* transcripts were identified either as individual entities or in small confluent clusters (Figs. 1, 2, and Additional file 1: Fig. S1), making it difficult to accurately count individual transcripts. Consequently, in this study, we relied on the

area density values of *SNCA* transcripts [25]. *SNCA* area density was determined by dividing the area occupied by *SNCA* transcripts by the annotated cell body area (ROI) and was displayed as the percentage. We analyzed *SNCA* transcripts area density in distinct cellular areas: (I) the total cell body, (II) the nucleus, and (III) the cytoplasm, which was calculated by (I) subtracting (II). In addition, we evaluated the cytoplasm without the LB area. In cells showing punctate α-syn IR we did not perform this evaluation. The individual measurement of *SNCA* area density from each cell was pooled into distinct morphological groups of inclusion types. The parameters used for image analysis were standardized and consistently applied throughout the entire experiment.

Pathological α-syn immunoreactive neurons were stratified as those with more than two small dot-like or threadlike immunostaining (so-called punctate α-syn IR) [33, 40, 73], and those with compact inclusions. Compact inclusions in the substantia nigra were further subclassified as irregular-shaped compact inclusions which did not correspond to the classical brainstem-type LB (bLB), and the classical bLB with a round core and pale halo [33, 40, 73]. In the amygdala, we distinguished punctate α-syn IR and compact inclusions identified as cortical-type LB (cLB) [33]. To quantify the nuclear area density of *SNCA* transcripts within neurons, astrocytes, and oligodendrocytes, an ROI encompassing the nucleus, visualized using DAPI staining, was meticulously delineated. This analysis was performed on neurons in the SN and amygdala, oligodendrocytes in the pons, and astrocytes in the amygdala using 2 control cases.

To quantify α-syn-IR neuritic pathology, serial sections of the SN used in the RNAscope study were immunostained with the 5G4 antibody, and then scanned using the TissueScope LE120 (Huron Digital Pathology, St. Jacobs, Canada). Subsequently the images were imported into HALO software (version 3.6, Indica Labs, Albuquerque, NM). The Object Colocalization module was employed for analysis. The SN was manually annotated, and an algorithm was established to exclusively quantify α-syn-IR neurites (see Additional file 1: Fig. S2). LBs and neurons containing neuromelanin were excluded mainly due to their size and optical density. The software calculated the percentage of α-syn-IR neurites positive area within the ROI. Detailed procedures used in the HALO analysis were provided in the Supplementary methods in Additional file 1.

snRNA-seq and data processing

snRNA-seq was performed as previously reported [25]. In brief, 3 control cases of frozen frontal cortex stored at -80℃ were chopped and loaded on Singulator TM 100 (S2 Genomics1). Small-volume nuclei isolation was
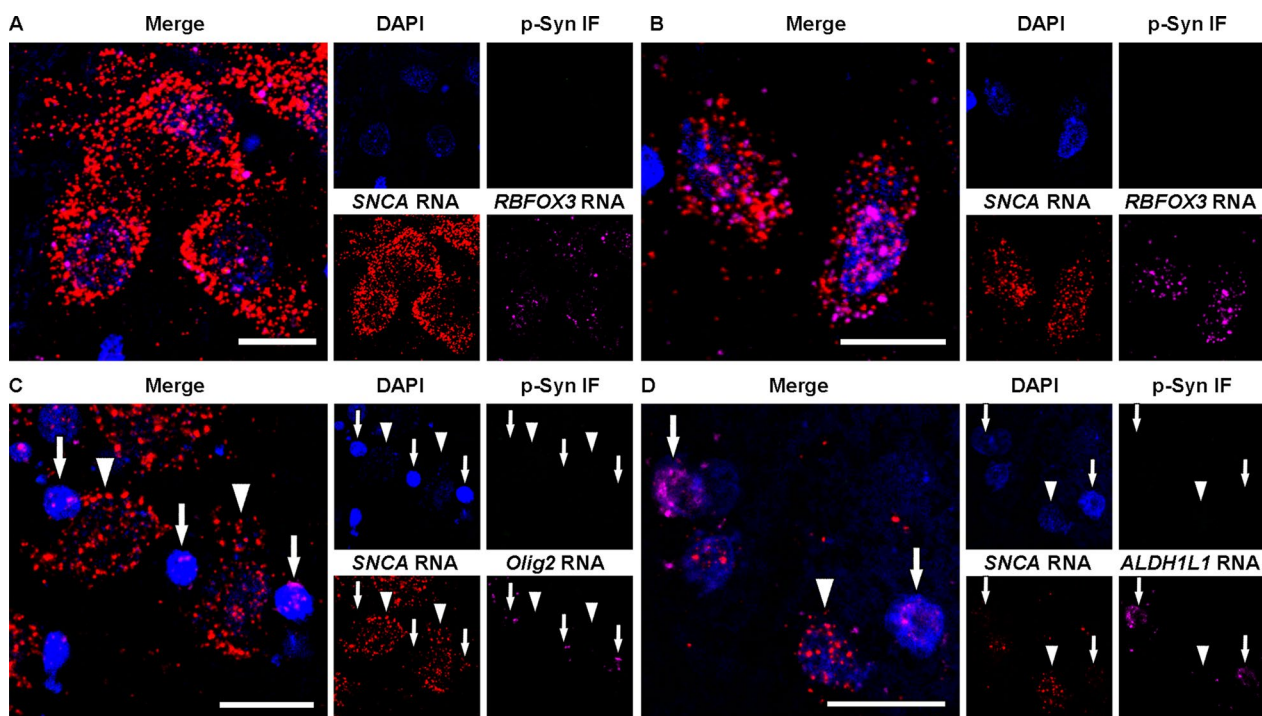
Fig. 1 Representative images of RNAscope combined with immunofluorescence in control cases. **A**, **B** Neurons in the substantia nigra (**A**) and amygdala (**B**) express numerous *SNCA* and neuron-specific *RBFOX3* transcripts in the nucleus and cytoplasm. **C** Oligodendrocytes contain many *Olig2* transcripts and few *SNCA* transcripts (arrows) whereas neurons exhibit numerous *SNCA* transcripts and an absence of *Olig2* transcripts (arrowheads). **D** Astrocytes contain many *ALDH1L1* transcripts and few *SNCA* transcripts (arrows) while neurons show numerous *SNCA* transcripts and an absence of *ALDH1L1* transcripts (arrowhead). Each image set represents confocal images taken from the same field of view showing DAPI (blue), phosphorylated-α-syn (p-Syn) immunofluorescence (green), *SNCA* (red), neuron-specific *RBFOX3* (**A**, **B**), oligodendrocytes-specific *Olig2* (**C**), or astrocyte-specific *ALDH1L1* (**D**, magenta), and the enlarged merged image. Note that in control cases p-Syn pathology is not detected. Scale bars represent 20 µm

performed using the Automated Tissue Dissociation System with minor adjustments. Singulator cartridges (S2 Genomics) were inserted with frozen tissues and mounted on the system for nuclei isolation. The collected nuclei were stained with DAPI and sorted using an Aria Fusion A cell sorter for DAPI-positive cells. The nuclei were stained with SYBR Green II and counted under a microscope using INCYTO C-Chip hemocytometers (Neubauer Improved). Sorted nuclei were used as input into the 10X Genomics single-cell 3' v3.1 assay and processed as 10X Genomics protocol and then the library was constructed. The quality of the library was assessed by Bioanalyzer (Agilent Technologies) and qPCR amplification data (Roche).

The single-nuclei transcriptome sequencing data were processed using the Cell Ranger Single-Cell Software Suite (v 6.0.0) from 10X Genomics. The raw data were demultiplexed to identify cell and unique molecular identifier (UMI) barcodes, followed by alignment to the GRCh38 reference genome using the STAR (v 2.7.10) tool available in the Cell Ranger pipeline. Gene expression quantification was combined into a single feature-barcode matrix. To normalize the depth across all merged datasets, the 'Cell Ranger aggr' function was utilized, ensuring a similar number of uniquely mapped transcriptome reads per cell.

Dimensionality reduction was performed using principal component analysis (PCA), with the top 10 principal components selected for subsequent analyses. Cells were clustered based on the k-means algorithm, and the results were visualized using UMAP (Uniform Manifold Approximation and Projection). Differentially expressed genes (DEGs) were identified using the Seurat FindConservedMarkers function ($p < 0.05$; negative binomial exact test). To assign cell types, known brain cell type markers [32] were mapped to the DEGs in each cluster. Three approaches were employed to assign cell type identity with stringent criteria. Initially, we created a graph showing the count of shared genes between known marker genes and cluster-specific top 50 differentially expressed genes in each cluster. Second, we generated a plot illustrating the average expression levels of marker genes that were differentially expressed across all clusters. Third, we calculated the average expression levels of the known
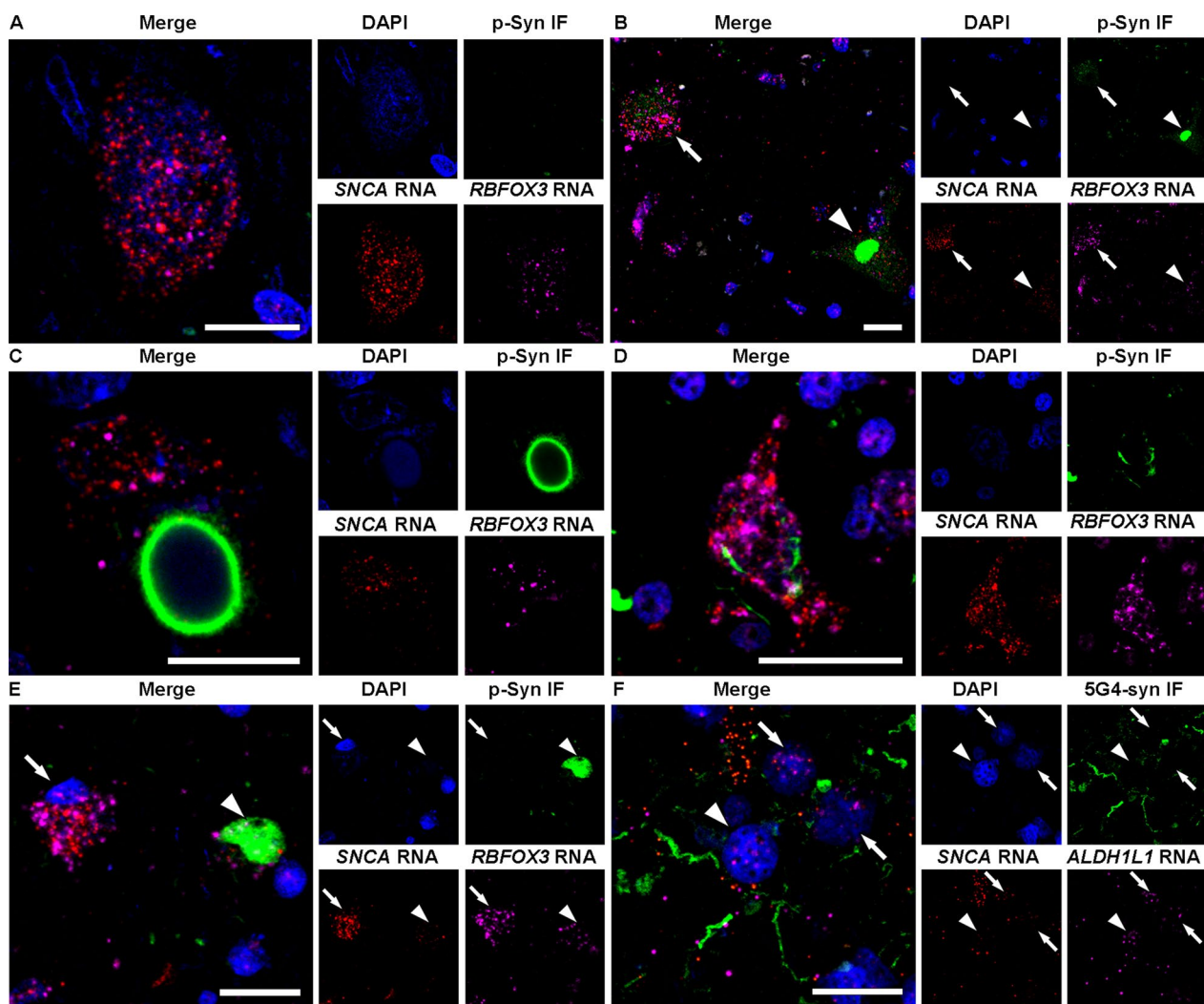
Fig. 2 Representative images of RNAscope combined with immunofluorescence in Lewy body disease cases. **A** A neuron without α-synuclein (α-syn) immunoreactivity (IR) in the substantia nigra, which has numerous *SNCA* and neuron-specific *RBFOX3* transcripts in the nucleus and cytoplasm. **B** Punctate α-syn IR (arrow) in a neuron, which shows many fine dots-like α-syn IR, and an irregular-shaped compact inclusion (arrowhead), which shows compact α-syn IR without a core or halo. Numerous *SNCA* transcripts are observed in the neuron containing the punctate α-syn IR compared with the neuron with irregular-shaped compact inclusion. **C** Brainstem-type Lewy body (bLB) containing a round core and pale halo shows few *SNCA* transcripts. **D**. A neuron containing a punctate α-syn IR in the amygdala shows numerous *SNCA* transcripts. **E**. A neuron without α-syn IR (arrow) and a cortical LB (cLB, arrowhead) in the amygdala show few *SNCA* transcripts. **F**. Astrocytes with (arrowhead) and without (arrows) α-syn IR in the amygdala contain few *SNCA* transcripts. Each image set represents confocal images taken from the same field of view showing phosphorylated-α-syn (p-Syn, **A**–**E**) or 5G4 α-syn (5G4-syn, **F**) immunostaining (green), *SNCA* (red), neuron-specific *RBFOX3* (**A**–**E**) or astrocyte-specific *ALDH1L1* (**F**, magenta), DAPI (blue), and the enlarged merged image. Scale bars represent 20 μm

marker genes in various clusters. Cell type identity was assigned to each cluster based on the restricted expression of marker genes, incorporating information from all three approaches. Heatmaps and boxplots were generated using the plotly package in Python.

Statistical analysis

Statistics were performed using GraphPad Prism (version 9) and SPSS Statistics Version 23. Kruskal–Wallis test and Dunn's post hoc analysis with Bonferroni correction were used to compare the area density of *SNCA* transcripts. The 10th percentile Z-score cut-off was calculated by Statology (https://www.statology.org/z-score-cut-off-calculator/) to determine the proportion of the area density of LBs below the 10th percentile of the neurons without α-syn IR [71]. If this proportion reached 50% of cells, we interpret this as a strong indicator for a decrease in SNCA transcript area density compared with

neurons without α-syn IR [25]. In addition, to account for potential case-specific variations and mitigate their influence, we conducted an analysis of covariance (ANCOVA) with each individual case and α-syn morphologies as the covariates. Pearson correlation analysis was applied between the percentage area of α-syn IR neurites and total cell body *SNCA* area density. Mann Whitney test with Bonferroni correction were used to compare the expression of *SNCA* using snRNA-seq data. Two-sided $p < 0.05$ was considered significant.

Results
Demographics and neuropathological data of cases
Demographics and neuropathological data of patients used in this study are summarized in Table 1. Age in LBD cases ranged from 62 to 85 (median 73) years at death, and control cases ranged from 52 to 77 (median 70) years at death. Postmortem interval in LBD cases ranged from 4 to 24 (median 15) hours, and control cases ranged from 4 to 30 (median 12.5) hours. Braak LBD stages in LBD were 4 and 5, and no Lewy pathology was observed in control cases. ADNC was intermediate in 2 cases of LBD, and absent in other cases.

RNAscope combined with immunostaining for α-syn
In the control cases (n = 2), *SNCA* transcripts were observed abundantly in the nucleus and cytoplasm in neurons in the SN, amygdala, and pons (Fig. 1A–C), while only single *SNCA* transcripts were found in the nucleus and cytoplasm in the oligodendrocytes in the pons (Fig. 1C) and in astrocytes in the amygdala (Fig. 1D). *SNCA* transcripts were clearly distinguishable from autofluorescence neuromelanin or lipofuscin particles (see Additional file 1: Fig. S1). In accordance with our previous report [38], transcripts of *RBFOX3*, *Olig2*, and *ALDH1L1* in neurons, oligodendrocytes, and astrocytes, respectively, were detected both in the cytoplasm and

nucleus in each cell type. Phosphorylated α-syn IR was not observed in the control cases.

In LBD cases, *SNCA* transcripts were also observed in the neuronal nucleus and cytoplasm (Fig. 2A,E) including those containing punctate α-syn IR (Fig. 2B,D), irregular-shaped compact inclusion (Fig. 2B), bLB (Fig. 2C), and cLB (Fig. 2E). However, *SNCA* transcripts were only rarely found in the α-syn immunoreactive LB areas (Fig. 2C,E; an additional video file shows this in more detail: Additional file 2). As reported previously, our investigations employing phosphorylated α-syn antibody failed to identify α-syn IR in astrocytes. Instead, we utilized the 5G4 α-syn antibody, known for its ability to detect disease-associated astrocytic α-syn IR [2, 9, 37, 39]. However, *SNCA* transcripts were infrequently observed both with and without disease-associated α-syn IR in astrocytes (Fig. 2F).

Quantification of SNCA transcripts in various α-syn cytopathologies
The total cell body *SNCA* area density was similar in pooled neurons without α-syn IR (n = 117 in the SN, median 17.1%; n = 305 in the amygdala, median 27.9%) and pooled neurons with punctate α-syn IR (n = 18 in the SN, median 13.8%; n = 37 in the amygdala, median 26.8%) (Fig. 3A,B). However, a gradual decrease of the total cell body *SNCA* area density in pooled neurons with irregular-shaped compact inclusions (n = 14, median 12.4%) followed by pooled bLBs (n = 17, median 5.6%) was observed, which showed statistical significance (neurons without α-syn IR vs bLB, p < 0.001; neurons with punctate α-syn IR vs bLB, $p = 0.01$) in the SN (Fig. 3A). Also, the total cell body area density of *SNCA* transcripts in pooled neurons with cLBs (n = 176, median 14.1%) was significantly lower than those without α-syn IR ($p < 0.001$) or with punctate α-syn IR (p < 0.001) in the amygdala (Fig. 3B). The significant statistical differences persisted even after applying ANCOVA (see Additional

(See figure on next page.)
Fig. 3 Area density of *SNCA* transcripts in neurons in the substantia nigra and amygdala. **A, B** Box and whisker plots of the total cell body *SNCA* transcripts area density in the substantia nigra (SN, **A**) and amygdala (**B**). *SNCA* transcript area density in neurons without disease-associated α-synuclein (α-syn) immunoreactivity (IR) in the SN (n = 117) and amygdala (n = 305) are similar to neurons with punctate disease-associated α-syn IR in the SN (n = 18) and amygdala (n = 37). However, *SNCA* transcript area density in neurons with irregular-shaped compact inclusions (n = 14), and those with brainstem-type Lewy bodies (bLB, n = 17) in the SN show a gradual decrease (**A**). The *SNCA* transcript area density in neurons containing cortical LB (cLB, n = 176) also shows a decrease compared to neurons without disease-associated α-syn IR and with disease-associated punctate α-syn IR (**B**). **C, D** Distribution of *SNCA* area density in neurons in the SN (**C**) and amygdala (**D**). Distribution curves of *SNCA* area density gradually deviate to a lower value during the maturation process of LBs. X-axis represents the area density expressed as the percentage and y-axis demonstrates the number of cells (Note that y-axis scales are different from **C** and **D**). While the nuclear *SNCA* transcript area density shows no differences (**E**), a significant decrease in cytoplasmic *SNCA* transcript area density is evident during LB maturation process in the SN (**F**). A significant decrease in *SNCA* transcript area density is also observed in the cytoplasmic area without compact inclusions and LB (**G**). The upper and lower whiskers indicate the 95th percentile and 5th percentile, respectively. The top and bottom of the box indicate the first and third quartiles, respectively. The middle line splitting the box indicates the median. The small circles in the plots indicate outliers. For statistics, Kruskal–Wallis test and Dunn's post hoc analysis with Bonferroni correction are used. Statistically significant findings where $p < 0.05$, $p < 0.01$, and $p < 0.001$ are indicated as *, **, and *** respectively
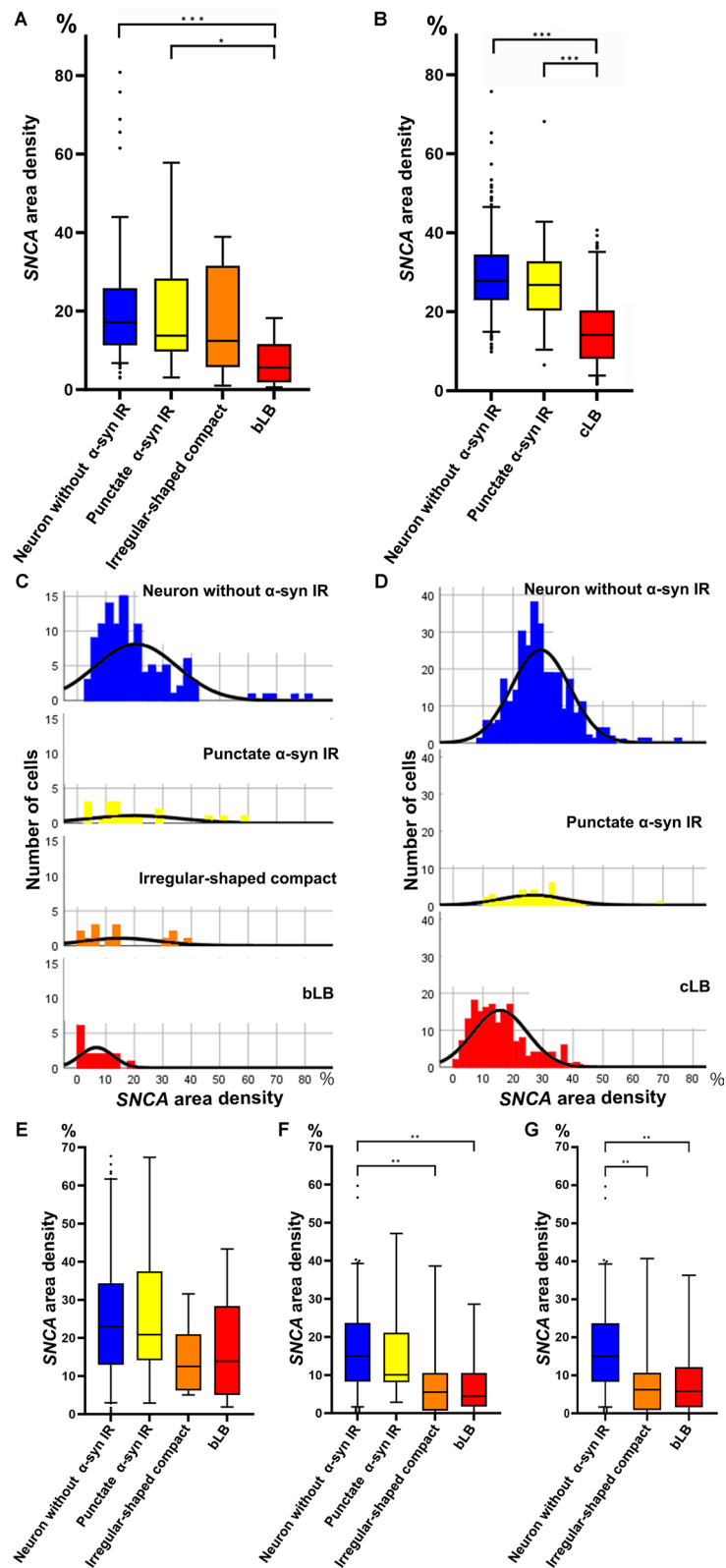
Fig. 3 (See legend on previous page.)

file 1: Table S2). Although the total cell body *SNCA* transcript area density varied between pooled neurons with and without α-syn IR, the distribution curves gradually deviated to the lower values during the maturation process of LB formation (Fig. 3C,D). Among the observed inclusions, 14.3% of irregular-shaped compact inclusions, 35.3% of bLBs, and 69.3% of cLBs fell below the 10th percentile Z-score cut-off of neurons without α-syn IR.

Since only a small number of *SNCA* transcripts were observed in LBs (see Additional file 2), we conducted an analysis of different parts of the cell body (i.e., nucleus and cytoplasm) to confirm the impact of LB occupancy on the reduction of *SNCA* transcripts observed in the total cell body. While the nuclear *SNCA* transcript area density remained unchanged (Fig. 3E), a decrease in cytoplasmic *SNCA* transcript area density was evident during LB maturation process, with statistically significant differences observed when comparing neurons without α-syn IR to neurons with irregular-shaped compact inclusions ($p = 0.001$) and bLB ($p = 0.003$) (Fig. 3F). Additionally, a decrease in *SNCA* transcript area density was also observed in the cytoplasmic area without the compact inclusions, with statistically significant differences when comparing neurons without α-syn IR to neurons with irregular-shaped compact inclusions ($p = 0.005$) and bLB ($p = 0.007$) (Fig. 3G).

Nuclear SNCA transcripts area density

We further quantified *SNCA* area density within the nucleus in neurons, oligodendrocytes, and astrocytes in control cases (n = 2) to compare with the results of snRNA-seq. We found that the nuclear area density of *SNCA* transcripts in pooled neurons (n = 101 in the SN, median 30.1%; n = 112 in the amygdala, median 37%) was significantly higher ($p < 0.001$) compared to pooled oligodendrocytes (n = 113, median 8.6%) and pooled astrocytes (n = 105, median 5.3%). Furthermore, the nuclear area density of *SNCA* transcripts in oligodendrocytes was significantly higher than that in astrocytes ($p < 0.05$). No statistically significant distinction in the nuclear *SNCA* transcripts area density was observed between neurons in the SN and amygdala (Fig. 4).

Cell-type specific SNCA expression in the frontal cortex

Based on our RNAscope analysis, we detected occasional *SNCA* transcripts in oligodendrocytes and astrocytes. This observation would add to the current incomplete understanding of α-syn expression in glial cells because α-syn is generally considered a neuronal protein [63, 64]. Therefore, we further conducted snRNA-seq analysis in control cases (n = 3). A comprehensive dataset comprising 15,265 transcriptome profiles from individual nuclei was successfully generated. The analysis revealed
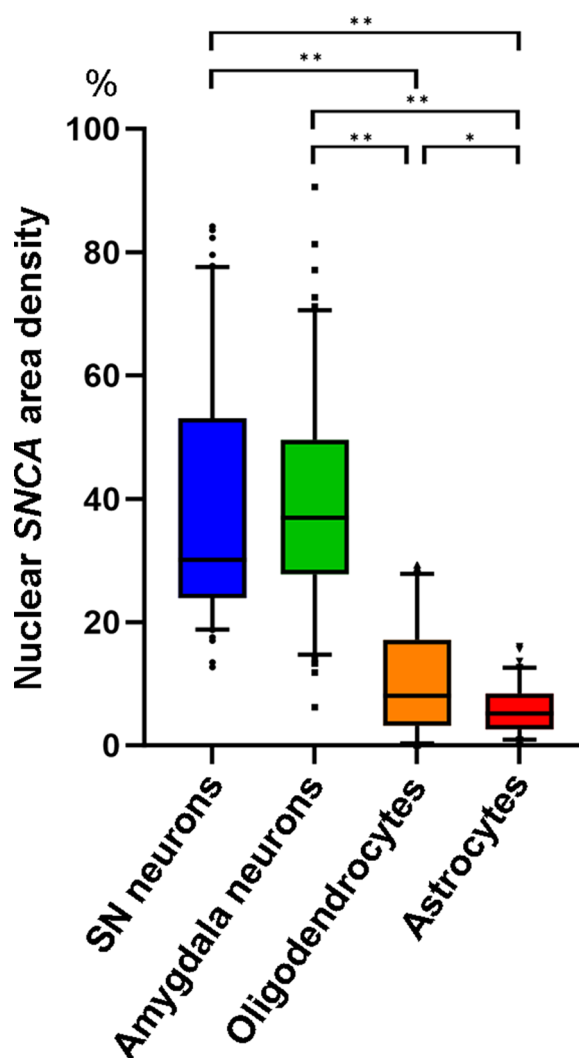

Fig. 4 Nuclear area density of *SNCA* transcripts in neurons, oligodendrocytes, and astrocytes in controls. Box and whisker plots of nuclear area density of *SNCA* transcript area density in neurons in the substantia nigra (SN, n = 101) and amygdala (n = 112), oligodendrocytes in the pons (n = 113), and astrocytes in the amygdala (n = 105) in control cases. The nuclear area density of *SNCA* transcripts in neurons is significantly higher than those in oligodendrocytes and astrocytes ($p < 0.001$). The nuclear area density of *SNCA* transcripts in oligodendrocytes is significantly higher than that of astrocytes ($p < 0.05$). The upper and lower whiskers indicate the 95th percentile and 5th percentile, respectively. The top and bottom of the box indicate the first and third quartiles, respectively. The middle line splitting the box indicates the median. The small circles in the plots indicate outliers. For statistics, Kruskal–Wallis test and Dunn's post hoc analysis with Bonferroni correction are used. Statistically significant findings where $p < 0.05$ and $p < 0.001$ are indicated as * and **, respectively

a median count of 8,007 unique molecular identifiers (UMIs) per cell, corresponding to a median detection of 2,998 genes per cell. We achieved an average

sequencing saturation of 88.8% for the libraries. Following this, we performed cluster annotation based on the expression of established marker genes associated with known cell types. Our snRNA-seq analysis uncovered a distinct pattern specific to each cell type (Fig. 5A). Notably, we observed a substantial expression of *SNCA* transcripts in homeostatic microglia, oligodendrocyte progenitor cells, and inhibitory neurons ($p = 4.4 \times 10^{-5}$ vs mature oligodendrocytes, $p = 4.8 \times 10^{-26}$ vs astrocytes). Conversely, we noted a low expression in excitatory neurons ($p = 7.3 \times 10^{-21}$ vs astrocytes) and mature oligodendrocytes ($p = $ vs 1.2×10^{-33} vs astrocytes). Moreover, the expression of *SNCA* transcripts was largely absent in astrocytes, microglia, and endothelial cells (Fig. 5B). It is noteworthy that the expression of the *SNCA* transcript is significantly higher in inhibitory neurons compared to excitatory neurons ($p = 3.3 \times 10^{-6}$).

Correlation of neuritic α-syn pathology and SNCA transcripts

The area density of α-syn-IR neurites in LBD cases using HALO ranged from 0.9% to 2.6% in the SN. Pearson correlation analysis between the percentage area of α-syn-IR neurites and the median value of the total cell *SNCA* transcripts area density in neurons without α-syn IR and bLB did not reveal any significant correlation. The correlation coefficient (r) between α-syn-IR neurites and *SNCA* transcripts in neurons without α-syn-IR was 0.18 ($p = 0.78$), and the r value between α-syn-IR neurites and *SNCA* transcripts in bLB was -0.23 ($p = 0.71$).

Immunohistochemistry for pan- and disease-associated-α-syn antibodies

To support literature data on preserved α-syn protein expression in LBD, we immunostained SN, striatum, and amygdala using an antibody that detects the physiological and disease-associated form of α-syn (SYN-1) and one that detects only the disease-associated α-syn (5G4). This confirmed preserved synaptic immunoreactivity in the striatum and SN for the antibody detecting the physiological form of α-syn in both non-diseased controls and LBD samples, while only LBD samples showed typical disease-associated α-syn deposits such as a dense neuritic and neuronal cytoplasmic pathology using the 5G4 antibody. For details see Additional file 1: Fig. S3.

Discussion

This study revealed preserved in early stages, but gradually decreasing, *SNCA* transcripts in the SN and amygdala neurons during the maturation process of LB formation.

'Proteinopathy' and 'proteinopenia', representing contrasting concepts, dictate divergent treatment strategies:

the elimination of disease-associated α-syn or the replacement of normal physiological α-syn early in the disease pathogenesis. *SNCA* transcripts in the SN in LBD have been reported to be both up- and down-regulated compared with controls [5, 7, 12, 14, 16, 28, 34, 53, 56, 60, 69]. The previous studies used a tissue-digested method that reported the average expression levels across a pool of neuronal and non-neuronal cell types. In contrast to these, increased *SNCA* transcripts in neuromelanin-containing neurons in the substantia nigra in Parkinson's disease compared with controls were reported using laser-microdissection and quantitative reverse transcription PCR [28]. Since mRNA expression can vary between cases and cells due to various reasons, our study did not focus on comparison of *SNCA* expression between controls and LBD cases, in particular, that we examined cases with developed stage of LBD where even normal-looking neurons might be different as in non-affected SN. Our study expands the findings of Grundemann et al., [28] who evaluated all neurons in the SN irrespective of α-syn pathology. Indeed, in contrast to our cytopathology-based evaluation, the approach of that study was not able to compare *SNCA* transcripts and α-syn pathology. The individual dots of RNAscope signal represents its expression level of transcripts [74]. However, *SNCA* transcripts appeared as isolated dots or in small confluent clusters, making it difficult to accurately count individual transcripts. Therefore, we used the area density measurements of *SNCA* transcripts as its expressional level in this study that reliably detects alterations in the transcripts [25].

Our RNAscope analysis revealed that *SNCA* transcripts within the total cell body and cytoplasm alone were preserved in punctate α-syn IR but significantly decreased in irregular-shaped compact inclusions and LBs, while they remained unchanged in the nucleus in all α-syn cytopathologies (Fig. 3). We found that the decline in *SNCA* transcripts is not simply a consequence of LB occupancy of the cytoplasm. We believe that this reflects most likely an exhaustion of the transcription due to the constant production of α-syn that is then utilized for the seeding of misfolded α-syn. This phenomenon would be reminiscent of the mechanism described in the leading model of neurodegenerative proteinopathies, which is associated with misfolded prion protein (PrP), wherein the progressive accumulation of misfolded PrP leads to a depletion of the pool of physiological cellular PrP [38]. Considering *SNCA* transcripts are rarely observed within the region of α-syn immunoreactive LB as observed through RNAscope, it can also be hypothesized that neurons are unable to generate *SNCA* transcripts due to the densely packed filaments that constitute the LBs' ultrastructural composition [18, 62, 73]. Finally, we cannot exclude the
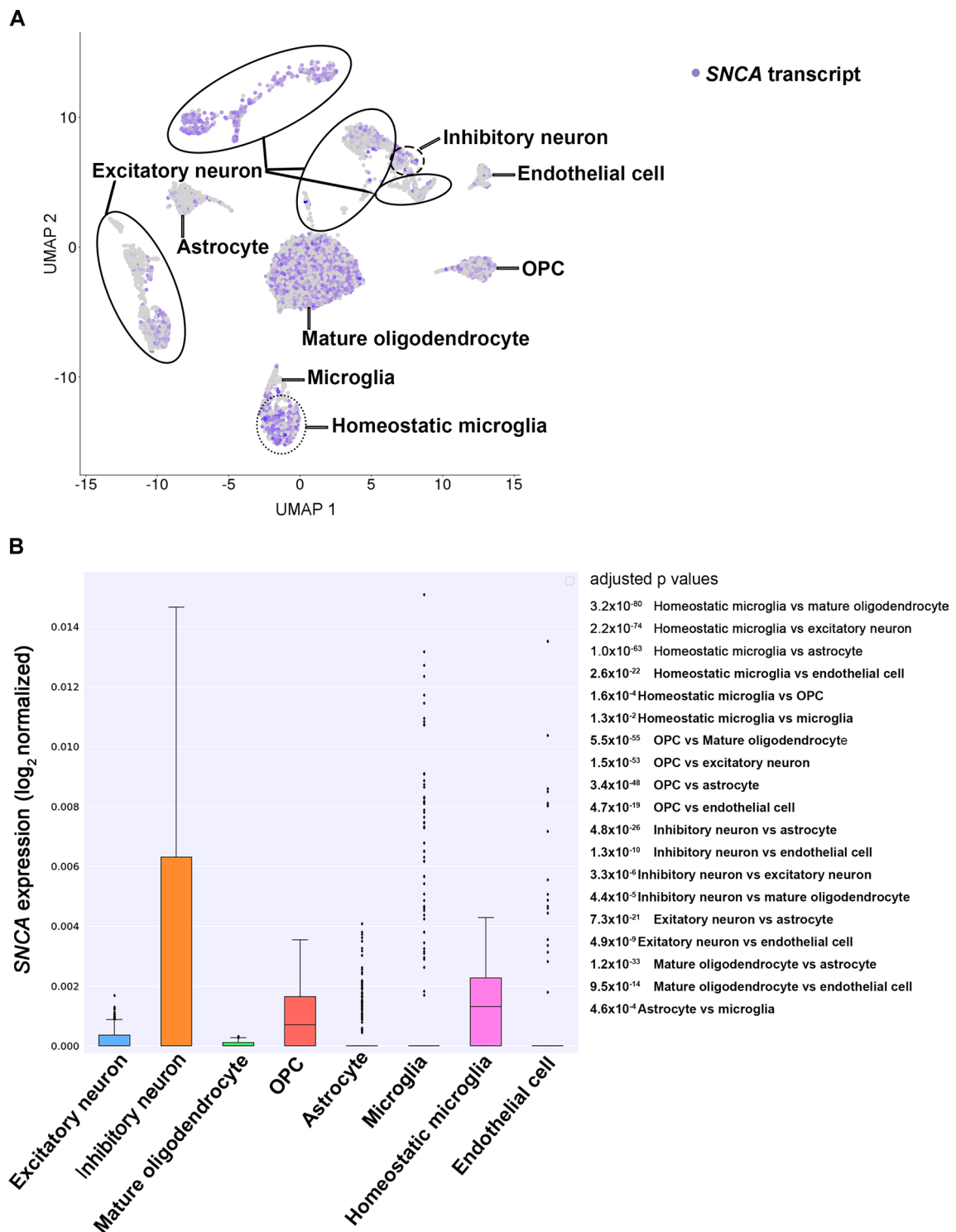
Fig. 5 *SNCA* expression in single-nucleus RNA sequencing in control cases **A** Expression profile of *SNCA* in major cell types of the control frontal cortex uncovering a distinct pattern specific to each cell type. Each point represents a single cell and color intensity indicates the normalized expression level of *SNCA*. UMAP projection of 15, 265 brain cells included. **B** Quantification of *SNCA* expression across cell types. The median of expression is depicted as a line within the box and whiskers indicate the range of the normalized *SNCA* expression. For statistics, Mann Whitney test with Bonferroni correction is used. Adjusted p values are listed on the right side of the figure. OPC, oligodendrocyte progenitor cell

possibility that the accumulation of misfolded α-syn during LB maturation exerts a negative feedback effect on the transcriptional regulation of *SNCA*.

We noted a variation in *SNCA* transcripts within morphologically distinct α-syn IR cytopathologies, with the mature LBs showing the least. This diversity in *SNCA* expression likely reflects a dynamic phenomenon in the human brain, as transcription at the cellular level undergoes continuous fluctuations in response to physiological or pathological demands. Similarly, protein expression of mitochondrial complex markers has been reported to differ between α-syn cytopathologies, supporting the concept that α-syn deposition is associated with dynamic cellular protein and RNA responses [24, 41].

A basic concept of molecular biology emphasizes that proteins are synthesized from mRNA templates [10]. Therefore, it is commonly observed that transcript expression levels correlate with protein synthesis [10, 23, 50, 58, 72]. However, the correlation of expression levels between mRNA and protein varies widely and its

abundance is imperfect [10, 29]. For example, targeted proteomics on a subset of proteins across cell lines and tissues yielded r values ranging from 0.39 to 0.79 [10, 19]. Regarding α-syn, over- and down-regulation of *SNCA* mRNA in cell culture and animal models correspond to the expression level of α-syn protein [66, 75]. Moreover, brains from patients with PD with *SNCA* triplication exhibited two-fold over-expression of *SNCA* mRNA and α-syn protein [23]. Interestingly, for another neurodegenerative disease-related protein, tau, the regional variability in total tau protein expression levels correlates with similar changes in mRNA expression levels evaluated with the quantitative RT-PCR method [72]. Indeed, and in line with previous studies using Western blots [30, 36, 39, 48], demonstrating preserved expression of monomeric α-syn in LBD samples, we also demonstrate preserved monomeric α-syn IR in the SN, striatum, and amygdala of LBD cases (Fig. S3).

Based on our observations we hypothesize the following scenario (Fig. 6). Neurons have a well-described
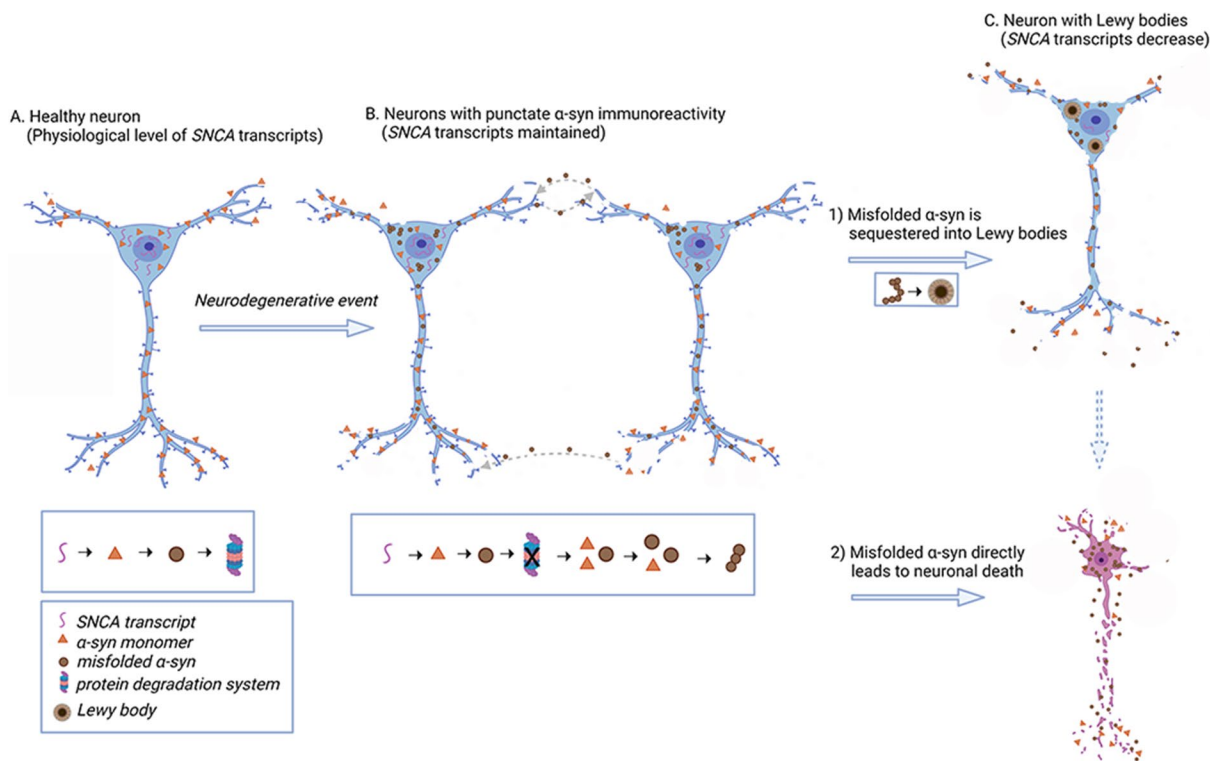

Fig. 6 Schematic hypothesis of cellular regulation of *SNCA* transcripts during the maturation process of Lewy body formation **A** In healthy condition, neurons express physiological levels of *SNCA* transcripts, and their protein degradation systems function normally. **B** When a "neurodegenerative event" occurs, (e.g. protein degradation system dysfunction) monomeric α-synuclein (α-syn) misfolds and serves as seeds for further disease propagation. Additionally, α-syn seeds are internalized from the extracellular space. Punctate α-syn immunoreactivity is observed in the cytoplasm in both cases. The neuron tries to 'sequester' misfolded α-syn. Due to the misfolding of α-syn, its physiological function is impaired. The neuron attempts to preserve physiological functioning by maintaining normal levels of *SNCA* transcripts. **C** Neurons reach a critical state and either (1) the misfolded α-syn is segregated into Lewy body, *SNCA* transcripts reduce due to cell dysfunction, ultimately leading to neuronal death, or, (2) the misfolded α-syn directly leads to neuronal death. Expression level of monomeric α-syn is preserved during the progression of the disease. Created with BioRender.com

maturation process of α-syn protein IR [33, 40, 73], driven also by posttranslational modifications affecting the amplification of disease-associated α-syn [75], which include punctate α-syn IR, irregular-shaped compact inclusion, and classical LBs [15, 27, 40, 54, 59, 73]. Neurons contain *SNCA* transcripts to serve as a pool for protein production. Following a "neurodegenerative event", monomeric α-syn misfolds, and serves as seeds for further disease propagation [27, 31, 35, 48, 49]. In addition, α-syn seeds are internalized from the extracellular space [27, 37]. Morphologically, an early cytopathological alteration reflecting this process is the punctate, non-ubiquitin positive, disease-associated α-syn IR. Parallelly to sequestering the misfolded α-syn leading to the formation of a LB, the neuron attempts to maintain normal levels of *SNCA* transcripts. At a certain stage, neurons reach a critical state and exhaust their cellular pool of *SNCA* transcripts, furthermore, they can no longer process the misfolded α-syn. Importantly, the *SNCA* transcription and physiological monomeric α-syn expression are preserved in the early stages of the maturation process of cytopathologies and not lost completely even at the later stages, as shown by the preserved physiological presynaptic α-syn staining and Western blot observations [30, 36, 39, 48].

Regarding astrocytes, the lack or very low-level of cellular production of *SNCA* strongly supports the notion that astrocytes ingest and not produce disease-associated α-syn themselves [11, 37, 44, 45]. This contrasts the development of astrocytic tau pathology where astrocytes can produce tau themselves that likely serves as a local pool for misfolding [25]. Whether astrocytic intake exerts a cytoprotective [44, 45] or cytotoxic [11, 43] mechanism cannot be answered in our study.

We infrequently observed *SNCA* transcripts in oligodendrocytes and astrocytes by RNAscope analysis. Nuclear *SNCA* area density in these glial cells was significantly lower than that of neurons, in addition, that of oligodendrocytes was significantly higher than astrocytes. Our snRNA-seq findings support the results, showing *SNCA* expression mostly in inhibitory neurons, OPCs, and homeostatic microglia, while low expression in excitatory neurons and mature oligodendrocytes. In contrast, *SNCA* transcripts were hardly detectable in astrocytes, microglia, and epithelial cells. Notably, *SNCA* transcript expression in inhibitory neurons was significantly higher than in excitatory neurons. In mice cultured cells, α-syn aggregate formation was observed in GAD-positive inhibitory neurons [67, 68]. Furthermore, α-syn positive inclusions were identified in medium spiny neurons, known for GABAergic inhibitory cells, in patients with PD [52]. Given that α-syn expression levels are directly associated with LB pathology [20], the enrichment of *SNCA* transcripts in specific neuronal cell types may influence their vulnerability to LB pathology. Oligodendrocytes, astrocytes, and microglia appear to express α-syn, but the level of expression is much lower than that in neurons [1, 3, 17, 57, 70]. We compared our *SNCA* transcripts expression dataset in snRNA-seq with 3 publicly available databases: (1) a human single-cell RNA-seq database, scRNAseqDB (https://bioinfo.uth.edu/scrnaseqdb/), (2) single cell RNAseq section in THE HUMAN PROTEIN ATLAS (HPA, https://www.proteinatlas.org/), (3) an immunopanning purification cell based RNA-Seq database, Brain RNA-Seq database (http://www.brainrnaseq.org, refers to an article [76]). Consistent with our dataset, we observed moderate to high *SNCA* transcript expression in neurons and OPCs, and low to moderate expression of *SNCA* transcripts in oligodendrocytes, while astrocytes exhibited low expression across all databases. However, there were variations in the expression levels of *SNCA* transcripts in microglia among the different databases. Our data exhibited higher expression of *SNCA* transcripts in homeostatic microglia, while low expression in microglia. Brain RNA-Seq showed moderate *SNCA* transcript expression in microglia, whereas both scRNAseqDB and HPA indicated low expression. *SNCA* transcript expression in homeostatic microglia was not accessible in these databases. Mice with *SNCA* overexpression exhibit microglial activation, which contributes to the degeneration of dopaminergic neurons [6]. The expression of *SNCA* transcripts may play a role in microglial cell activation/differentiation and contribute to neurodegenerative processes. Notably, our data was obtained through single 'nucleus' RNA-seq, whereas the other databases utilized single 'cell' RNA-seq methodologies. Therefore, our study highlights nuclear *SNCA* transcripts expression can be different from cytoplasm or whole-cell transcripts. By employing snRNA-seq, it has been revealed that *SNCA* is not limited to dopaminergic neurons but is also expressed in other neurons, oligodendrocytes, and homeostatic microglia. This observation challenges the conventional notion of α-syn as exclusively a neuronal protein [3], shedding light on its expression in glial cells. The significance of *SNCA* transcript expression underlying the formation of oligodendroglial cytoplasmic inclusions, which serve as a distinctive pathological feature of multiple system atrophy (MSA), is emphasized. We highlight our ongoing efforts to investigate the expression of *SNCA* in oligodendroglial cytoplasmic inclusions in MSA, aiming to provide further insights into the disease.

It is important to note that this study has some limitations. Detailed morphometric evaluations can be performed on only a small number of cases. However, the cytopathologies were well represented and the preserved *SNCA* transcripts were clear in all. In addition, the model of progressive α-syn aggregation observed through immunohistochemistry may not be universally applicable and may exhibit certain exceptions. Furthermore, we did not assess the expression of *SNCA* transcripts in specific cell lineages, such as dopaminergic neurons or GABAergic neurons. This is because the RNAscope method used here does not allow the application of a wide range of neuronal markers. Importantly, we focused on neuromelanin-containing cells of the substantia nigra that are dopaminergic. Finally, although our study supports literature data on the preserved presynaptic staining of physiological α-syn and shows preserved *SNCA* transcription in cells during the cytopathological process, we did not measure the solubility of proteins that is a focus of the proteinopenia theory [22].

Conclusions

Our study revealed preserved *SNCA* transcription in substantia nigra and amygdala neurons in early maturation stages of α-syn-related cytopathologies that gradually decreases during the formation of LBs. Our study advances our understanding of the pathogenesis of LBD by elucidating the upstream regulation of *SNCA* expression during disease progression and uncovering cell-type specific diversity of *SNCA* expression. We highlight novel aspects of disease pathogenesis that will be relevant for basic researchers working on cellular mechanisms of synucleinopathies.

Abbreviations

α-syn	α-Synuclein
ACD	Advanced cell diagnostics
ADNC	Alzheimer's disease neuropathological change
ALDH1L1	Aldehyde dehydrogenase 1 family member L
bLB	Brainstem-type Lewy body
cLB	Cortical-type Lewy body
DAPI	4′,6-Diamidino-2-phenylindole
DEG	Differentially expressed gene
HPA	HUMAN PROTEIN ATLAS
IHC	Immunohistochemistry
IR	Immunoreactivity
LB	Lewy body
LBD	Lewy body disease
MSA	Multiple system atrophy
Olig2	Oligodendrocyte transcription factor 2
OPCs	Oligodendrocyte progenitor cells
PCA	Principal component analysis
PCR	Polymerase chain reaction
RBFOX3	RNA Binding Fox-1 Homolog 3
ROI	Region of interest
SN	Substantia nigra
SNCA	α-Synuclein gene
snRNA-seq	Single nucleus RNA sequencing
UMAP	Uniform manifold approximation and projection
UMI	Unique molecular identifier

Supplementary Information

The online version contains supplementary material available at https://doi.org/10.1186/s40478-023-01687-7.

Additional file 1: **Fig. S1**. Method of outlining the region of interest and capturing the positive signals in RNAscope. Raw data image of the SN section in a case of Lewy body disease (**A**). Lookup Table strength of the cell-specific marker and DAPI channels are increased enough to make the level of autofluorescence of neuromelanin and/or lipofuscin pigments visible (**B**). Then, the cell body borders are traced by their signals as total cell area (**C**). DAPI channel is selected and the nuclear edge is outlined as the nucleus area (**D**). Phosphorylated-α-syn immunostaining channel is represented in green and selected. The edge of LB is drawn as LB area (**E**). Subsequently, returning the LUT parameters to the default settings, positive signals corresponding to SNCA transcripts above the threshold within the region of interest are captured by the NIS-Elements software (**F**). Red displays SNCA transcripts, magenta shows RBFOX3 transcripts, and blue exhibits DAPI. Scale bar represents 10 μm. **Fig. S2**. Method of outlining the region of interest and capturing synuclein-immunoreactive neurites in HALO. The SN, region of interest, is demarcated by a yellow line (**A**). A magnified view of the boxed area in A is presented in (**B**), with the captured area highlighted in red (**C**). **Fig. S3**. Immunohistochemistry for SYN-1 and 5G4 α-synuclein (α-syn) antibodies. SYN-1 antibody cross-reacts with the physiological monomeric α-syn and shows a synaptic pattern in both cases of controls (**A**, **C**, **E**, **G**) and LBD (**B**, **D**, **F**, **H**) in addition to revealing Lewy body and related pathology in the diseased substantia nigra (SN, **D**) and putamen (**F**). In contrast, the 5G4 antibody does not label the physiological synaptic staining in the SN and putamen in cases of control (**C**, **G**) nor of LBD (**D**, **H**) and highlights only the disease associated α-syn immunoreactivity in LBD (**D**, **H**). Immunostaining for SYN-1 (**A**, **B**, **E**, **F**) and 5G4 (**C**, **D**, **G**, **H**) anti-α-syn antibodies in the SN (**A**–**D**) and putamen (**E**–**H**). The scale bars represent 50 μm for each image.

Additional file 2: 3D RNAscope imaging of a classical Lewy body SNCA transcripts are rarely observed within phosphorylated-α-syn immunoreactive Lewy body areas. Green represents phosphorylated-α-syn immunostaining, red displays SNCA transcripts, magenta shows RBFOX3 transcripts, and blue exhibits DAPI. See additional video file.

Author contributions

TK carried out the RNAscope and IHC experiments, analyzed and interpreted the data, and drafted the manuscript. SLF conducted the IHC experiment, analyzed and interpreted the data, and edited the manuscript. SL performed the RNAscope and snRNA-seq experiments, analyzed and interpreted the data, and edited the manuscript. IMV carried out the snRNA-seq experiment, interpreted the data, and edited the manuscript. JL conducted the RNAscope and IHC experiments and edited the manuscript. NN performed the snRNA-seq experiment and analyzed and interpreted the data, and edited the manuscript. MJU carried out the snRNA-seq experiment, analyzed and interpreted the data, and edited the manuscript. AEL interpreted the data and edited the manuscript. GGK conceptualized the study, conducted the RNAscope and IHC experiments, analyzed and interpreted the data, and edited the manuscript. All authors read and approved the final manuscript.

Availability of data and materials

The datasets used and analysed during the current study are available from the corresponding author on reasonable request.

Declarations

Ethics approval and consent to participate

This study was approved by the University Health Network (UHN) Research Ethics Board (Nr. 20-5258) and the University of Toronto (Nr. 39459) and was performed per ethical standards established in the 1964 Declaration of Helsinki, updated in 2008.

Consent for publication

Not applicable.

Competing interests

GGK holds shared patent for the 5G4 antibody. All other authors declare that they have no competing interests regarding this study.

Author details

[1]Tanz Centre for Research in Neurodegenerative Disease, University of Toronto, 60 Leonard Ave., Rm 6KD414, Tanz CRND, Krembil Discovery Tower, Toronto, ON M5T 0S8, Canada. [2]Department of Neurology, Hirosaki University Graduate School of Medicine, Hirosaki, Japan. [3]Dementia Research Centre, Macquarie Medical School, Faculty of Medicine, Health and Human Sciences, Macquarie University, Sydney, Australia. [4]Laboratory Medicine Program and Krembil Brain Institute, University Health Network, Toronto, ON, Canada. [5]College of Medicine, Mohammed Bin Rashid University of Medicine and Health Sciences, Dubai, UAE. [6]GenomeArc Inc, Toronto, ON, Canada. [7]Edmund J Safra Program in Parkinson's Disease and Rossy Progressive Supranuclear Palsy Centre, Toronto Western Hospital, Toronto, ON, Canada. [8]Department of Medicine, Division of Neurology, University of Toronto, Toronto, ON, Canada. [9]Department of Laboratory Medicine and Pathobiology, University of Toronto, Toronto, ON, Canada.

References

1. Agarwal D, Sandor C, Volpato V, Caffrey TM, Monzon-Sandoval J, Bowden R et al (2020) A single-cell atlas of the human substantia nigra reveals cell-specific pathways associated with neurological disorders. Nat Commun 11:4183. https://doi.org/10.1038/s41467-020-17876-0
2. Altay MF, Liu AKL, Holton JL, Parkkinen L, Lashuel HA (2022) Prominent astrocytic alpha-synuclein pathology with unique post-translational modification signatures unveiled across Lewy body disorders. Acta Neuropathol Commun 10:163. https://doi.org/10.1186/s40478-022-01468-8
3. Asi YT, Simpson JE, Heath PR, Wharton SB, Lees AJ, Revesz T et al (2014) Alpha-synuclein mRNA expression in oligodendrocytes in MSA. Glia 62:964–970. https://doi.org/10.1002/glia.22653
4. Attems J, Toledo JB, Walker L, Gelpi E, Gentleman S, Halliday G et al (2021) Neuropathological consensus criteria for the evaluation of Lewy pathology in post-mortem brains: a multi-centre study. Acta Neuropathol 141:159–172. https://doi.org/10.1007/s00401-020-02255-2
5. Beyer K, Lao JI, Carrato C, Mate JL, Lopez D, Ferrer I et al (2004) Differential expression of alpha-synuclein isoforms in dementia with Lewy bodies. Neuropathol Appl Neurobiol 30:601–607. https://doi.org/10.1111/j.1365-2990.2004.00572.x
6. Bido S, Muggeo S, Massimino L, Marzi MJ, Giannelli SG, Melacini E et al (2021) Microglia-specific overexpression of alpha-synuclein leads to severe dopaminergic neurodegeneration by phagocytic exhaustion and oxidative toxicity. Nat Commun 12:6237. https://doi.org/10.1038/s41467-021-26519-x
7. Borrageiro G, Haylett W, Seedat S, Kuivaniemi H, Bardien S (2018) A review of genome-wide transcriptomics studies in Parkinson's disease. Eur J Neurosci 47:1–16. https://doi.org/10.1111/ejn.13760
8. Braak H, Del Tredici K, Rub U, de Vos RA, Jansen Steur EN, Braak E (2003) Staging of brain pathology related to sporadic Parkinson's disease. Neurobiol Aging 24:197–211. https://doi.org/10.1016/s0197-4580(02)00065-9
9. Braak H, Sastre M, Del Tredici K (2007) Development of alpha-synuclein immunoreactive astrocytes in the forebrain parallels stages of intra-neuronal pathology in sporadic Parkinson's disease. Acta Neuropathol 114:231–241. https://doi.org/10.1007/s00401-007-0244-3
10. Buccitelli C, Selbach M (2020) mRNAs, proteins and the emerging principles of gene expression control. Nat Rev Genet 21:630–644. https://doi.org/10.1038/s41576-020-0258-4
11. Cavaliere F, Cerf L, Dehay B, Ramos-Gonzalez P, De Giorgi F, Bourdenx M et al (2017) In vitro alpha-synuclein neurotoxicity and spreading among neurons and astrocytes using Lewy body extracts from Parkinson disease brains. Neurobiol Dis 103:101–112. https://doi.org/10.1016/j.nbd.2017.04.011
12. Chiba-Falek O, Lopez GJ, Nussbaum RL (2006) Levels of alpha-synuclein mRNA in sporadic Parkinson disease patients. Mov Disord 21:1703–1708. https://doi.org/10.1002/mds.21007
13. Chu Y, Muller S, Tavares A, Barret O, Alagille D, Seibyl J et al (2019) Intrastriatal alpha-synuclein fibrils in monkeys: spreading, imaging and neuropathological changes. Brain 142:3565–3579. https://doi.org/10.1093/brain/awz296
14. Dachsel JC, Lincoln SJ, Gonzalez J, Ross OA, Dickson DW, Farrer MJ (2007) The ups and downs of alpha-synuclein mRNA expression. Mov Disord 22:293–295. https://doi.org/10.1002/mds.21223
15. Desplats P, Lee HJ, Bae EJ, Patrick C, Rockenstein E, Crews L et al (2009) Inclusion formation and neuronal cell death through neuron-to-neuron transmission of alpha-synuclein. Proc Natl Acad Sci U S A 106:13010–13015. https://doi.org/10.1073/pnas.0903691106
16. Dijkstra AA, Ingrassia A, de Menezes RX, van Kesteren RE, Rozemuller AJ, Heutink P et al (2015) Evidence for immune response, axonal dysfunction and reduced endocytosis in the substantia Nigra in early stage Parkinson's disease. PLoS ONE 10:e0128651. https://doi.org/10.1371/journal.pone.0128651
17. Djelloul M, Holmqvist S, Boza-Serrano A, Azevedo C, Yeung MS, Goldwurm S et al (2015) Alpha-synuclein expression in the oligodendrocyte lineage: an in vitro and in vivo study using rodent and human models. Stem Cell Reports 5:174–184. https://doi.org/10.1016/j.stemcr.2015.07.002
18. Duffy PE, Tennyson VM (1965) Phase and electron micromicroscopic observations of Lewy bodies and melanin granules in the substantia nigra and locus caeruleus in Parkinson's disease. J Neuropathol Exp Neurol 24:398–414
19. Edfors F, Danielsson F, Hallstrom BM, Kall L, Lundberg E, Ponten F et al (2016) Gene-specific correlation of RNA and protein levels in human cells and tissues. Mol Syst Biol 12:883
20. Erskine D, Patterson L, Alexandris A, Hanson PS, McKeith IG, Attems J et al (2018) Regional levels of physiological alpha-synuclein are directly associated with Lewy body pathology. Acta Neuropathol 135:153–154. https://doi.org/10.1007/s00401-017-1787-6
21. Espay AJ, Okun MS (2023) Abandoning the proteinopathy paradigm in Parkinson disease. JAMA Neurol 80:123–124. https://doi.org/10.1001/jamaneurol.2022.4193
22. Ezzat K, Sturchio A, Espay AJ (2023) The shift to a proteinopenia paradigm in neurodegeneration. Handb Clin Neurol 193:23–32. https://doi.org/10.1016/B978-0-323-85555-6.00001-1
23. Farrer M, Kachergus J, Forno L, Lincoln S, Wang DS, Hulihan M et al (2004) Comparison of kindreds with parkinsonism and alpha-synuclein genomic multiplications. Ann Neurol 55:174–179. https://doi.org/10.1002/ana.10846
24. Flones IH, Nyland H, Sandnes DA, Alves GW, Tysnes OB, Tzoulis C (2022) Early forms of alpha-synuclein pathology are associated with neuronal complex I deficiency in the substantia Nigra of individuals with Parkinson's disease. Biomolecules. https://doi.org/10.3390/biom12060747
25. Forrest SL, Lee S, Nassir N, Martinez-Valbuena I, Sackmann V, Li J et al (2023) Cell-specific MAPT gene expression is preserved in neuronal and glial tau cytopathologies in progressive supranuclear palsy. Acta Neuropathol 146:395–414. https://doi.org/10.1007/s00401-023-02604-x
26. Fujishiro H, Imamura AY, Lin WL, Uchikado H, Mark MH, Golbe LI et al (2013) Diversity of pathological features other than Lewy bodies in familial Parkinson's disease due to SNCA mutations. Am J Neurodegener Dis 2:266–275

Kon *et al. Acta Neuropathologica Communications*   (2023) 11:185

Page 16 of 17

27. Goedert M, Spillantini MG, Del Tredici K, Braak H (2013) 100 years of Lewy pathology. Nat Rev Neurol 9:13–24. https://doi.org/10.1038/nrneurol.2012.242

28. Grundemann J, Schlaudraff F, Haeckel O, Liss B (2008) Elevated alpha-synuclein mRNA levels in individual UV-laser-microdissected dopaminergic substantia nigra neurons in idiopathic Parkinson's disease. Nucleic Acids Res 36:e38. https://doi.org/10.1093/nar/gkn084

29. Gry M, Rimini R, Stromberg S, Asplund A, Ponten F, Uhlen M et al (2009) Correlations between RNA and protein expression profiles in 23 human cell lines. BMC Genomics 10:365. https://doi.org/10.1186/1471-2164-10-365

30. Hasegawa M, Fujiwara H, Nonaka T, Wakabayashi K, Takahashi H, Lee VM et al (2002) Phosphorylated alpha-synuclein is ubiquitinated in alpha-synucleinopathy lesions. J Biol Chem 277:49071–49076. https://doi.org/10.1074/jbc.M208046200

31. Holec SAM, Liu SL, Woerman AL (2022) Consequences of variability in alpha-synuclein fibril structure on strain biology. Acta Neuropathol 143:311–330. https://doi.org/10.1007/s00401-022-02403-w

32. Hu C, Li T, Xu Y, Zhang X, Li F, Bai J et al (2023) Cell Marker 2.0: an updated database of manually curated cell markers in human/mouse and web tools based on scRNA-seq data. Nucleic Acids Res 51:D870–D876. https://doi.org/10.1093/nar/gkac947

33. Katsuse O, Iseki E, Marui W, Kosaka K (2003) Developmental stages of cortical Lewy bodies and their relation to axonal transport blockage in brains of patients with dementia with Lewy bodies. J Neurol Sci 211:29–35. https://doi.org/10.1016/s0022-510x(03)00037-6

34. Kingsbury AE, Daniel SE, Sangha H, Eisen S, Lees AJ, Foster OJ (2004) Alteration in alpha-synuclein mRNA expression in Parkinson's disease. Mov Disord 19:162–170. https://doi.org/10.1002/mds.10683

35. Kon T, Tomiyama M, Wakabayashi K (2020) Neuropathology of Lewy body disease: clinicopathological crosstalk between typical and atypical cases. Neuropathology 40:30–39. https://doi.org/10.1111/neup.12597

36. Koss DJ, Erskine D, Porter A, Palmoski P, Menon H, Todd OGJ et al (2022) Nuclear alpha-synuclein is present in the human brain and is modified in dementia with Lewy bodies. Acta Neuropathol Commun 10:98. https://doi.org/10.1186/s40478-022-01403-x

37. Kovacs GG, Breydo L, Green R, Kis V, Puska G, Lorincz P et al (2014) Intracellular processing of disease-associated alpha-synuclein in the human brain suggests prion-like cell-to-cell spread. Neurobiol Dis 69:76–92. https://doi.org/10.1016/j.nbd.2014.05.020

38. Kovacs GG, Voigtlander T, Hainfellner JA, Budka H (2002) Distribution of intraneuronal immunoreactivity for the prion protein in human prion diseases. Acta Neuropathol 104:320–326. https://doi.org/10.1007/s00401-002-0550-8

39. Kovacs GG, Wagner U, Dumont B, Pikkarainen M, Osman AA, Streichenberger N et al (2012) An antibody with high reactivity for disease-associated alpha-synuclein reveals extensive brain pathology. Acta Neuropathol 124:37–50. https://doi.org/10.1007/s00401-012-0964-x

40. Kuusisto E, Parkkinen L, Alafuzoff I (2003) Morphogenesis of Lewy bodies: dissimilar incorporation of alpha-synuclein, ubiquitin, and p62. J Neuropathol Exp Neurol 62:1241–1253. https://doi.org/10.1093/jnen/62.12.1241

41. Lang A, Dassler E, Milenkovic I, Lutz MI, Kovacs GG (2021) Variable expression of mitochondrial complex IV in the course of nigral intracellular accumulation of alpha-synuclein. Parkinsonism Relat Disord 90:57–61. https://doi.org/10.1016/j.parkreldis.2021.08.001

42. Lang AE, Siderowf AD, Macklin EA, Poewe W, Brooks DJ, Fernandez HH et al (2022) Trial of cinpanemab in early Parkinson's disease. N Engl J Med 387:408–420. https://doi.org/10.1056/NEJMoa2203395

43. Lee HJ, Suk JE, Patrick C, Bae EJ, Cho JH, Rho S et al (2010) Direct transfer of alpha-synuclein from neuron to astroglia causes inflammatory responses in synucleinopathies. J Biol Chem 285:9262–9272. https://doi.org/10.1074/jbc.M109.081125

44. Lindstrom V, Gustafsson G, Sanders LH, Howlett EH, Sigvardson J, Kasrayan A et al (2017) Extensive uptake of alpha-synuclein oligomers in astrocytes results in sustained intracellular deposits and mitochondrial damage. Mol Cell Neurosci 82:143–156. https://doi.org/10.1016/j.mcn.2017.04.009

45. Loria F, Vargas JY, Bousset L, Syan S, Salles A, Melki R et al (2017) alpha-Synuclein transfer between neurons and astrocytes indicates that astrocytes play a role in degradation rather than in spreading. Acta Neuropathol 134:789–808. https://doi.org/10.1007/s00401-017-1746-2

46. Luk KC, Song C, O'Brien P, Stieber A, Branch JR, Brunden KR et al (2009) Exogenous alpha-synuclein fibrils seed the formation of Lewy body-like intracellular inclusions in cultured cells. Proc Natl Acad Sci U S A 106:20051–20056. https://doi.org/10.1073/pnas.0908005106

47. Maroteaux L, Campanelli JT, Scheller RH (1988) Synuclein: a neuron-specific protein localized to the nucleus and presynaptic nerve terminal. J Neurosci 8:2804–2815. https://doi.org/10.1523/JNEUROSCI.08-08-02804.1988

48. Martinez-Valbuena I, Swinkin E, Santamaria E, Fernandez-Irigoyen J, Sackmann V, Kim A et al (2022) alpha-Synuclein molecular behavior and nigral proteomic profiling distinguish subtypes of Lewy body disorders. Acta Neuropathol 144:167–185. https://doi.org/10.1007/s00401-022-02453-0

49. Martinez-Valbuena I, Visanji NP, Kim A, Lau HHC, So RWL, Alshimemeri S et al (2022) Alpha-synuclein seeding shows a wide heterogeneity in multiple system atrophy. Transl Neurodegener 11:7. https://doi.org/10.1186/s40035-022-00283-4

50. Miller DW, Hague SM, Clarimon J, Baptista M, Gwinn-Hardy K, Cookson MR et al (2004) Alpha-synuclein in blood and brain from familial Parkinson disease with SNCA locus triplication. Neurology 62:1835–1838. https://doi.org/10.1212/01.wnl.0000127517.33208.f4

51. Montine TJ, Phelps CH, Beach TG, Bigio EH, Cairns NJ, Dickson DW et al (2012) National Institute on Aging-Alzheimer's Association guidelines for the neuropathologic assessment of Alzheimer's disease: a practical approach. Acta Neuropathol 123:1–11. https://doi.org/10.1007/s00401-011-0910-3

52. Mori F, Tanji K, Zhang H, Kakita A, Takahashi H, Wakabayashi K (2008) alpha-Synuclein pathology in the neostriatum in Parkinson's disease. Acta Neuropathol 115:453–459. https://doi.org/10.1007/s00401-007-0316-4

53. Neystat M, Lynch T, Przedborski S, Kholodilov N, Rzhetskaya M, Burke RE (1999) Alpha-synuclein expression in substantia nigra and cortex in Parkinson's disease. Mov Disord 14:417–422. https://doi.org/10.1002/1531-8257(199905)14:3%3c417::aid-mds1005%3e3.0.co;2-x

54. Osterberg VR, Spinelli KJ, Weston LJ, Luk KC, Woltjer RL, Unni VK (2015) Progressive aggregation of alpha-synuclein and selective degeneration of lewy inclusion-bearing neurons in a mouse model of parkinsonism. Cell Rep 10:1252–1260. https://doi.org/10.1016/j.celrep.2015.01.060

55. Pagano G, Taylor KI, Anzures-Cabrera J, Marchesi M, Simuni T, Marek K et al (2022) Trial of prasinezumab in early-stage Parkinson's disease. N Engl J Med 387:421–432. https://doi.org/10.1056/NEJMoa2202867

56. Papapetropoulos S, Adi N, Mash DC, Shehadeh L, Bishopric N, Shehadeh L (2007) Expression of alpha-synuclein mRNA in Parkinson's disease. Mov Disord 22:1057–1059. https://doi.org/10.1002/mds.21466

57. Richter-Landsberg C, Gorath M, Trojanowski JQ, Lee VM (2000) alpha-synuclein is developmentally expressed in cultured rat brain oligodendrocytes. J Neurosci Res 62:9–14. https://doi.org/10.1002/1097-4547(20001001)62:1%3c9::AID-JNR2%3e3.0.CO;2-U

58. Riederer P, Berg D, Casadei N, Cheng F, Classen J, Dresel C et al (2019) alpha-Synuclein in Parkinson's disease: Causal or bystander? J Neural Transm 126:815–840. https://doi.org/10.1007/s00702-019-02025-9

59. Roberti MJ, Bertoncini CW, Klement R, Jares-Erijman EA, Jovin TM (2007) Fluorescence imaging of amyloid formation in living cells by a functional, tetracysteine-tagged alpha-synuclein. Nat Methods 4:345–351. https://doi.org/10.1038/nmeth1026

60. Rockenstein E, Hansen LA, Mallory M, Trojanowski JQ, Galasko D, Masliah E (2001) Altered expression of the synuclein family mRNA in Lewy body and Alzheimer's disease. Brain Res 914:48–56. https://doi.org/10.1016/s0006-8993(01)02772-x

61. Rossi M, Candelise N, Baiardi S, Capellari S, Giannini G, Orru CD et al (2020) Ultrasensitive RT-QuIC assay with high sensitivity and specificity for Lewy body-associated synucleinopathies. Acta Neuropathol 140:49–62. https://doi.org/10.1007/s00401-020-02160-8

62. Roy S, Wolman L (1969) Ultrastructural observations in Parkinsonism. J Pathol 99:39–44. https://doi.org/10.1002/path.1710990106

63. Sorrentino ZA, Giasson BI, Chakrabarty P (2019) alpha-Synuclein and astrocytes: tracing the pathways from homeostasis to neurodegeneration in Lewy body disease. Acta Neuropathol 138:1–21. https://doi.org/10.1007/s00401-019-01977-2

64. Stefanova N, Wenning GK (2023) Multiple system atrophy: at the cross-roads of cellular, molecular and genetic mechanisms. Nat Rev Neurosci 24:334–346. https://doi.org/10.1038/s41583-023-00697-7

65. Suvarna V, Deshmukh K, Murahari M (2022) miRNA and antisense oligonucleotide-based alpha-synuclein targeting as disease-modifying therapeutics in Parkinson's disease. Front Pharmacol 13:1034072. https://doi.org/10.3389/fphar.2022.1034072

66. Tagliafierro L, Chiba-Falek O (2016) Up-regulation of SNCA gene expression: implications to synucleinopathies. Neurogenetics 17:145–157. https://doi.org/10.1007/s10048-016-0478-0

67. Taguchi K, Watanabe Y, Tsujimura A, Tanaka M (2019) Expression of alpha-synuclein is regulated in a neuronal cell type-dependent manner. Anat Sci Int 94:11–22. https://doi.org/10.1007/s12565-018-0464-8

68. Taguchi K, Watanabe Y, Tsujimura A, Tatebe H, Miyata S, Tokuda T et al (2014) Differential expression of alpha-synuclein in hippocampal neurons. PLoS ONE 9:e89327. https://doi.org/10.1371/journal.pone.0089327

69. Tan EK, Chandran VR, Fook-Chong S, Shen H, Yew K, Teoh ML et al (2005) Alpha-synuclein mRNA expression in sporadic Parkinson's disease. Mov Disord 20:620–623. https://doi.org/10.1002/mds.20391

70. Tanji K, Mori F, Nakajo S, Imaizumi T, Yoshida H, Hirabayashi T et al (2001) Expression of beta-synuclein in normal human astrocytes. NeuroReport 12:2845–2848. https://doi.org/10.1097/00001756-200109170-00018

71. Thomann AE, Berres M, Goettel N, Steiner LA, Monsch AU (2020) Enhanced diagnostic accuracy for neurocognitive disorders: a revised cut-off approach for the Montreal Cognitive Assessment. Alzheimers Res Ther 12:39. https://doi.org/10.1186/s13195-020-00603-8

72. Trabzuni D, Wray S, Vandrovcova J, Ramasamy A, Walker R, Smith C et al (2012) MAPT expression and splicing is differentially regulated by brain region: relation to genotype and implication for tauopathies. Hum Mol Genet 21:4094–4103. https://doi.org/10.1093/hmg/dds238

73. Wakabayashi K, Tanji K, Mori F, Takahashi H (2007) The Lewy body in Parkinson's disease: molecules implicated in the formation and degradation of alpha-synuclein aggregates. Neuropathology 27:494–506. https://doi.org/10.1111/j.1440-1789.2007.00803.x

74. Wang F, Flanagan J, Su N, Wang LC, Bui S, Nielson A et al (2012) RNAscope: a novel in situ RNA analysis platform for formalin-fixed, paraffin-embedded tissues. J Mol Diagn 14:22–29. https://doi.org/10.1016/j.jmoldx.2011.08.002

75. Zhang S, Zhu R, Pan B, Xu H, Olufemi MF, Gathagan RJ et al (2023) Post-translational modifications of soluble alpha-synuclein regulate the amplification of pathological alpha-synuclein. Nat Neurosci 26:213–225. https://doi.org/10.1038/s41593-022-01239-7

76. Zhang Y, Sloan SA, Clarke LE, Caneda C, Plaza CA, Blumenthal PD et al (2016) Purification and characterization of progenitor and mature human astrocytes reveals transcriptional and functional differences with mouse. Neuron 89:37–53. https://doi.org/10.1016/j.neuron.2015.11.013

Publisher's Note